Journal of Non-Newtonian Fluid Mechanics 212 (2014) 80–91

Contents lists available at ScienceDirect

Journal of Non-Newtonian Fluid Mechanics

journal homepage: http://www.elsevier.com/locate/jnnfm

Annular flow of viscoelastic fluids: Analytical and numerical solutions

L.L. Ferrás [a,*], A.M. Afonso [b], M.A. Alves [b], J.M. Nóbrega [a], F.T. Pinho [c]

[a] Institute for Polymers and Composites/I3N, University of Minho, Campus de Azurém, 4800-058 Guimarães, Portugal
[b] Departamento de Engenharia Química, CEFT, Faculdade de Engenharia da Universidade do Porto, Rua Dr. Roberto Frias s/n, 4200-465 Porto, Portugal
[c] Centro de Estudos de Fenómenos de Transporte, Faculdade de Engenharia da Universidade do Porto, Rua Dr. Roberto Frias s/n, 4200-465 Porto, Portugal

ARTICLE INFO

Article history:
Received 25 September 2013
Received in revised form 14 July 2014
Accepted 22 July 2014
Available online 7 August 2014

Keywords:
Annular flow
Analytical solution
sPTT model
Slip boundary conditions

ABSTRACT

This work provides analytical and numerical solutions for the linear, quadratic and exponential Phan–Thien–Tanner (PTT) viscoelastic models, for axial and helical annular fully-developed flows under no slip and slip boundary conditions, the latter given by the linear and nonlinear Navier slip laws. The rheology of the three PTT model functions is discussed together with the influence of the slip velocity upon the flow velocity and stress fields. For the linear PTT model, full analytical solutions for the inverse problem (unknown velocity) are devised for the linear Navier slip law and two different slip exponents. For the linear PTT model with other values of the slip exponent and for the quadratic PTT model, the polynomial equation for the radial location (β) of the null shear stress must be solved numerically. For both models, the solution of the direct problem is given by an iterative procedure involving three nonlinear equations, one for β, other for the pressure gradient and another for the torque per unit length. For the exponential PTT model we devise a numerical procedure that can easily compute the numerical solution of the pure axial flow problem.

1. Introduction

Annular flows are frequent in drilling operations, cable coating, or even in the food industry. In such flows, the presence of polymers with high molecular weight chains, together with rock cuttings, oil, mud and other solid particles, creates the perfect environment for wall slip to occur. It is not difficult to imagine a drilling operation where the drilling mud contains macromolecules generating a viscoelastic suspension of particles that slips along the wall. Therefore, this study presents a detailed analytical and numerical study of viscoelastic concentric annular flow with inner cylinder rotation with and without the presence of slip. For the viscoelastic fluids we use the linear, quadratic and exponential PTT models [1,2], and for the slip boundary conditions the linear and nonlinear Navier slip laws were chosen [3,4].

In the literature, we can find experimental work and analytical solutions for annular flows of viscoelastic and inelastic viscous fluids. Two particularly relevant works were published by Escudier et al. [5,6], who studied numerically and experimentally the fully developed laminar flow of purely viscous non-Newtonian liquids through annuli, including the effects of eccentricity and inner-cylinder rotation. An extensive literature review for inelastic fluids is also given in [5].

Just a few works could be found in the literature regarding analytical solutions for generalized Newtonian fluid flows in annular ducts and under slip. These are the works of Mathews and Hill [7] that presents analytical solutions for pipe, annular and channel Newtonian flows with the slip boundary conditions given by Thompson and Troian [8] (nonlinear Navier boundary condition), and by Kalyon and Malik [9] presenting analytical solutions for the Hershel–Bulkley, Bingham plastic, power-law, and Newtonian fluids with and without wall slip (true or apparent) at one or both surfaces of the annulus. They also concluded that their analytical solution could be used to tailor the processability of viscoplastic fluids in annular flows. Chatzimina et al. [10] presented a study on the stability of the annular Poiseuille flow of a Newtonian fluid assuming slip along the walls. They used different slip models relating the wall shear stress to the slip velocity (including non-monotonic slip models), and provided a partial explanation for the absence of the stick–slip instability in annular extrusion experiments (which is a major step for the empirical/theoretical understanding of such phenomenon).

For viscoelastic fluids the literature is, however, scarcer. Kulshrestha [11] studied the helical flow of a viscoelastic liquid described by the upper-convected Maxwell model, and presents analytical expressions for the velocity profiles, stresses and pressure gradient. Bhatnagar [12] investigated the steady laminar flow

* Corresponding author.
E-mail addresses: luis.ferras@dep.uminho.pt (L.L. Ferrás), aafonso@fe.up.pt (A.M. Afonso), mmalves@fe.up.pt (M.A. Alves), mnobrega@dep.uminho.pt (J.M. Nóbrega), fpinho@fe.up.pt (F.T. Pinho).

http://dx.doi.org/10.1016/j.jnnfm.2014.07.004
0377-0257/

of a viscoelastic fluid described by the Rivlin–Eriksen model through a pipe and through an annulus with suction or injection at the walls, and Ballal and Rivlin [13,14] considered the longitudinal flow of a viscoelastic fluid (second-order and fourth-order Rivlin–Ericksen constitutive equation) in the annular region between two eccentric cylinders of circular cross-section, and studied the flow resulting from the motion of the inner cylinder parallel to its axis (with constant velocity), with the outer cylinder being held fixed. They calculated the resultant forces on the cylinders, as well as the distribution of their normal and tangential components. Later, they extended the study performed on the second-order Rivlin–Ericksen constitutive equation: first, they assumed rotating cylinders [15], and then, they studied the problem in which both cylinders are stationary and the flow results from a uniform constant longitudinal pressure gradient [16]. Beris et al. [17] derived the circumferential and radial profiles of velocity, pressure and stress for the flow of viscoelastic liquids (Criminale–Ericksen–Filbey, upper-convected Maxwell and White–Metzner models) between two slightly eccentric cylinders with the inner one rotating. More recently, Pinho and Oliveira [18] presented an analytical solution for axial flow of the linear PTT model with no slip boundary conditions, which consists of the kinematic and stress profiles across the radial gap of a concentric annular flow in fully developed conditions. Subsequently, Cruz and Pinho [19] devised analytical solutions for the helical flow of the linear PTT fluid in concentric annuli, due to inner cylinder rotation, as well as for the skewed Couette–Poiseuille flow in a channel due to the movement of one of the plates in the spanwise direction, where they present expressions for the radial variation of the axial and tangential velocities, as well as for the shear and normal stresses.

Wood [20] provided analytical solutions for the transient viscoelastic helical flow, due to the combined action of rotating cylinders and a constant pressure gradient, in pipes of circular and annular cross-sections for a fluid modeled by the Oldroyd-B constitutive model. Jamil and Fetecau [21] presented a similar study for the upper-convected Maxwell fluid, with torsional and longitudinal time dependent shear stresses applied to the inner cylinder, extending the work by Bandelli and Rajagopal [22]. Wang and Xu [23] derived analytical solutions for the unsteady axial Couette flow of a fractional second grade fluid and fractional Maxwell fluid between two infinitely long concentric circular cylinders (see also [24,25] for more helical flows using fractional derivative models). Other works in the literature with viscoelastic fluids in annular geometries are mostly numerical, using Finite Volume or Finite Element methods to solve the complete system of equations [26–32] but are frequently concerned with the extrudate swell or coating flows. These simulations are usually computationally demanding, therefore analytical solutions are a powerful tool to investigate the flow behavior in simplified arrangements.

The results for viscoelastic helical fluid flow that were found in the literature, are almost all based on Oldroyd-B fluids or Maxwell fluids. Therefore, we are interested in extending these works to other fluid models. To do this, based on the works by Pinho and Oliveira [18] and Cruz and Pinho [19], we developed analytical/numerical solutions for fluids modeled by the quadratic and exponential sPTT constitutive equations, together with slip boundary conditions.

In this work, although some of the solutions obtained are numerical, we provide the codes that can be used to compute such solutions, allowing a fast access to the desired results. The codes can be downloaded from http://paginas.fe.up.pt/~fpinho/research/menur.html. The idea is to provide a friendly way to compute the solutions with almost the same cost as an analytical solution.

The remainder of this paper is organized as follows: we first present the governing equations for the three viscoelastic models in Section 2; Section 3 presents the analytical and numerical solutions; Section 4 discusses the results, and the paper ends with the conclusions in Section 5.

2. Governing equations

The isothermal and incompressible fluid flow considered in this work is governed by the continuity and the momentum equations,

$$\nabla \cdot \mathbf{u} = 0 \tag{1}$$

$$\rho \frac{\partial \mathbf{u}}{\partial t} + \rho \nabla \cdot \mathbf{uu} = -\nabla p + \nabla \cdot \boldsymbol{\tau} \tag{2}$$

where $\mathbf{u}$ is the velocity vector, p is the pressure, ρ is the density and $\boldsymbol{\tau}$ is the deviatoric stress tensor, given by the simplified Phan–Thien–Tanner (sPTT) model [1,2],

$$f(tr\boldsymbol{\tau})\boldsymbol{\tau} + \lambda\left(\frac{\partial \boldsymbol{\tau}}{\partial t} + \mathbf{u}\cdot\nabla\boldsymbol{\tau} - \left[(\nabla\mathbf{u})^T\cdot\boldsymbol{\tau} + \boldsymbol{\tau}\cdot\nabla\mathbf{u}\right]\right) = \eta\left(\nabla\mathbf{u} + (\nabla\mathbf{u})^T\right) \tag{3}$$

where η is the polymer viscosity coefficient, λ is the relaxation time of the fluid and $f(tr\boldsymbol{\tau})$ is a function of the trace of the extra-stress tensor specifying the various versions of this class of models [1,2],

$$f(tr\boldsymbol{\tau}) = \begin{cases} 1 + \frac{\varepsilon\lambda}{\eta}\tau_{kk} & \text{linear} \\ 1 + \frac{\varepsilon\lambda}{\eta}\tau_{kk} + \frac{1}{2}\left(\frac{\varepsilon\lambda}{\eta}\tau_{kk}\right)^2 & \text{quadratic} \\ \exp\left(\frac{\varepsilon\lambda}{\eta}\tau_{kk}\right) & \text{exponential} \end{cases} \tag{4}$$

The linear and exponential versions of the sPTT model are frequently used in the literature [33], but we also consider in this work a quadratic version, which is a second-order expansion of the exponential model, and therefore it is expected to lead to results in-between the linear and the exponential models. Since the quadratic model is not commonly used, we present in Fig. 1 the dimensionless material properties in steady shear flow of the three versions of the sPTT model considered in this work. To obtain these material functions, we consider a steady-state Couette flow in the x-direction, $\mathbf{u} = (\dot{\gamma}y, 0, 0)$, where $\dot{\gamma}$ is the shear rate. For this ideal flow the constitutive equation reduces to:

$$\begin{cases} f(tr\boldsymbol{\tau})\tau_{xx} = 2\lambda\dot{\gamma}\tau_{xy} \\ f(tr\boldsymbol{\tau})\tau_{xy} = \eta\dot{\gamma} \\ \tau_{yy} = \tau_{zz} = \tau_{xz} = \tau_{yz} = 0 \end{cases} \tag{5}$$

The relation between the shear stress and the normal stress is given by,

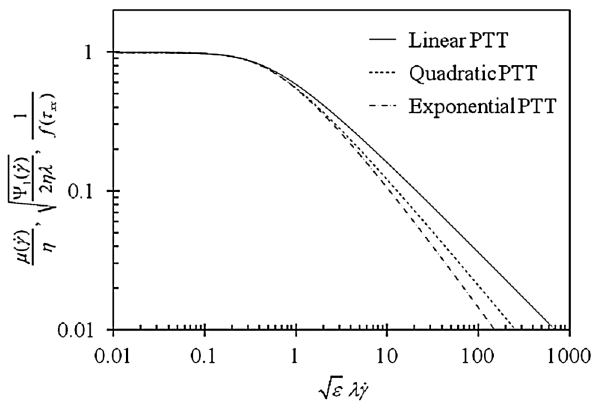

Fig. 1. Dimensionless material properties in steady-state Couette flow for the three versions of the sPTT model.

$$\tau_{xx} = 2\frac{\lambda}{\eta}\tau_{xy}^2 \tag{6}$$

The viscometric viscosity and the first normal stress difference coefficient can be written in the form (note that $tr\boldsymbol{\tau} = \tau_{xx}$):

$$\frac{\mu(\dot{\gamma})}{\eta} = \frac{\tau_{xy}}{\eta\dot{\gamma}} = \frac{1}{f(\tau_{xx})} \tag{7}$$

$$\frac{\Psi_1}{2\eta\lambda} = \frac{\tau_{xx}}{2\eta\lambda\dot{\gamma}^2} = \frac{1}{[f(\tau_{xx})]^2} \tag{8}$$

respectively. For the linear PTT model, Azaiez et al. [34] presented explicit functions for $f(tr\boldsymbol{\tau})$:

$$f(\tau_{xx}) = 1 + \frac{\left(B^{1/3} - 1\right)^2}{3B^{1/3}} \tag{9}$$

with $B = \left[1 + 27\varepsilon(\lambda\dot{\gamma})^2\right] + \sqrt{\left[1 + 27\varepsilon(\lambda\dot{\gamma})^2\right]^2 - 1}$.

The previous equations clearly illustrate that the dimensionless material functions depend on the generalized Deborah number $\sqrt{\varepsilon}(\lambda\dot{\gamma})$. For the quadratic and exponential PTT models, the dimensionless material functions are also a function of $\sqrt{\varepsilon}(\lambda\dot{\gamma})$ as shown in Fig. 1, but, to obtain their material functions we need to solve the non-linear system of equations (Eq. (5)), which can be written in terms of τ_{xx} in the following non-linear form:

$$\frac{1}{2}[f(\tau_{xx})]^2\frac{\lambda\varepsilon}{\eta}\tau_{xx} = \varepsilon(\lambda\dot{\gamma})^2 \tag{10}$$

By setting different values of $\frac{\lambda\varepsilon}{\eta}\tau_{xx}$ allows the direct calculation of $\sqrt{\varepsilon}(\lambda\dot{\gamma})$ using (10), and the function $f(\tau_{xx})$ is also directly computed, which allows the calculation of the material functions (Eqs. (7) and (8)), as shown in Fig. 1.

Two empirical wall boundary conditions were chosen for this problem, namely the classical no-slip condition (usually accepted as a law)

$$\mathbf{u} = \mathbf{0} \tag{11}$$

and the nonlinear Navier slip boundary condition [3,4] (the operator $\mathbf{w}_{tg} = \mathbf{w} - (\mathbf{w}\cdot\mathbf{n})\mathbf{n}$ gives the wall tangent vector),

$$\left\|\mathbf{u}_{tg}\right\| = k\left\|(\boldsymbol{\tau}\mathbf{n})_{tg}\right\|^m, \quad m > 0 \tag{12}$$

where $\mathbf{u}_{tg}$ is the wall slip velocity vector that points in the tangent stress opposite direction, $\mathbf{n}$ is the wall normal vector, k is the friction coefficient and $\|\cdot\|$ stands for the usual l^2-norm.

3. Annular flow analysis

3.1. Linear and quadratic PTT models

For this problem we assume the flow between two concentric cylinders is fully developed, with the axial velocity component, u, in the z-direction and the tangential velocity, v, only depending on the radial coordinate, r. We assume the stationary outer cylinder has a radius R, and the radius of the rotating inner cylinder (constant angular velocity, ω) is αR, with $0 < \alpha < 1$ (see Fig. 2).

Under these assumptions the simplified momentum equations are given by,

$$\frac{1}{r}\frac{\mathrm{d}(r\tau_{rz})}{\mathrm{d}r} = p_{,z} \tag{13}$$

$$-\rho\frac{v^2}{r} = \frac{1}{r}\frac{\mathrm{d}(r\tau_{rr})}{\mathrm{d}r} - \frac{\tau_{\theta\theta}}{r} - \frac{\mathrm{d}p}{\mathrm{d}r} \tag{14}$$

$$\frac{\mathrm{d}(r^2\tau_{r\theta})}{\mathrm{d}r} = 0 \tag{15}$$

and the constitutive equation simplifies to,

$$\begin{aligned}
&\tau_{rr} = 0 && (a) && \tau_{r\theta} = \tfrac{r\eta}{f(tr\boldsymbol{\tau})}\tfrac{\mathrm{d}(v/r)}{\mathrm{d}r} && (d)\\
&\tau_{zz} = \tfrac{2\lambda\eta}{[f(tr\boldsymbol{\tau})]^2}\left(\tfrac{\mathrm{d}u}{\mathrm{d}r}\right)^2 && (b) && \tau_{rz} = \tfrac{\eta}{f(tr\boldsymbol{\tau})}\tfrac{\mathrm{d}u}{\mathrm{d}r} && (e)\\
&\tau_{\theta\theta} = \tfrac{2\lambda\eta}{[f(tr\boldsymbol{\tau})]^2}\left(r\tfrac{\mathrm{d}(v/r)}{\mathrm{d}r}\right)^2 && (c) && \tau_{\theta z} = \tfrac{2\lambda\eta r}{[f(tr\boldsymbol{\tau})]^2}\tfrac{\mathrm{d}u}{\mathrm{d}r}\tfrac{\mathrm{d}(v/r)}{\mathrm{d}r} && (f)
\end{aligned} \tag{16}$$

where $p_{,z}$ is the imposed constant axial pressure gradient and z, r, θ stand for the longitudinal, radial and azimuthal directions, respectively. For more details see [19].

Following the procedure adopted by Cruz and Pinho [19] the following expressions are obtained for the extra stress components,

$$\begin{aligned}
&\tau_{rr} = 0 && (a) && \tau_{r\theta} = \tfrac{M}{2\pi r^2} && (d)\\
&\tau_{zz} = \tfrac{2\lambda}{\eta}\left[\tfrac{p_{,z}r}{2} + \tfrac{c_a}{r}\right]^2 && (b) && \tau_{rz} = \tfrac{p_{,z}r}{2} + \tfrac{c_a}{r} && (e)\\
&\tau_{\theta\theta} = \tfrac{\lambda M^2}{2\pi^2\eta r^4} && (c) && \tau_{\theta z} = \tfrac{\lambda M}{\pi r^2\eta}\left[\tfrac{p_{,z}r}{2} + \tfrac{c_a}{r}\right] && (f)
\end{aligned} \tag{17}$$

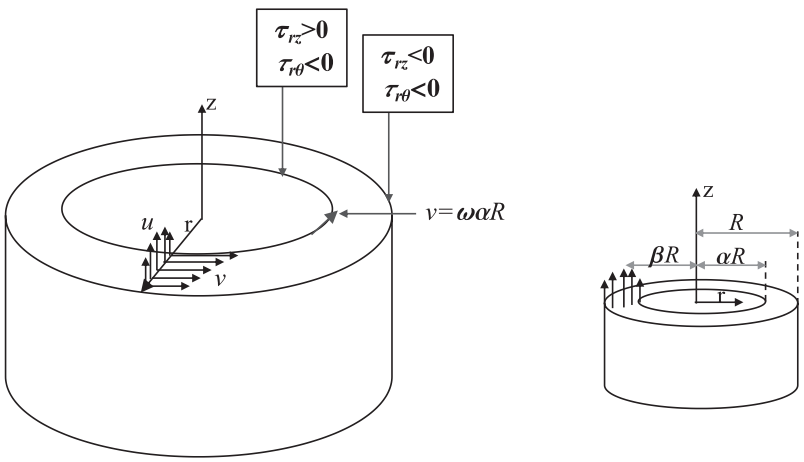

Fig. 2. Schematic of the annular flow.

where M is the torque per unit length and c_a is an integration constant.

Assuming that $\tau_{rz}=0$ at $r=\beta R$ (Fig. 2), with $\alpha<\beta<1$, the shear stress in the longitudinal direction is then given by,

$$\tau_{rz}=-\frac{p_{,z}\beta R}{2}\left(\frac{\beta R}{r}-\frac{r}{\beta R}\right). \tag{18}$$

The axial and tangential velocity gradients are given for the linear ($\chi=0$) and quadratic ($\chi=1$) PTT models by (the exponential model will only be analyzed for pure axial flow below),

$$\frac{\mathrm{d}(\bar{v}/\bar{r})}{\mathrm{d}\bar{r}}=\frac{U_T}{U}\frac{1}{2\bar{r}^3}\left\{1+2\varepsilon De^2\left[\frac{\bar{p}_{,z}\beta\bar{R}}{2}\left(\frac{\beta\bar{R}}{\bar{r}}-\frac{\bar{r}}{\beta\bar{R}}\right)\right]^2+\frac{\varepsilon De_T^2}{2\bar{r}^4}+\frac{1}{2}\chi\left(2\varepsilon De^2\left[\frac{\bar{p}_{,z}\beta\bar{R}}{2}\left(\frac{\beta\bar{R}}{\bar{r}}-\frac{\bar{r}}{\beta\bar{R}}\right)\right]^2+\frac{\varepsilon De_T^2}{2\bar{r}^4}\right)^2\right\} \tag{22}$$

The radial profiles of the axial and tangential velocities can be obtained from integration of Eqs. (21) and (22), respectively, and are given in a dimensionless form as, $\bar{u}(\bar{r})=\bar{u}_a(\bar{r})+\bar{c}_b$ and $\bar{v}(\bar{r})=\bar{r}\bar{v}_r(\bar{r})+\bar{c}_c\bar{r}$, with

$$\begin{aligned}\bar{u}_a(\bar{r})=&\frac{\chi\varepsilon^2De^4\bar{p}_{,z}^5\left(2\bar{r}^{10}-15\beta^2\bar{r}^8\bar{R}^2+60\beta^4\bar{r}^6\bar{R}^4-120\beta^6\bar{r}^4\bar{R}^6\ln(\bar{r})-30\beta^8\bar{r}^2\bar{R}^8+3\beta^{10}\bar{R}^{10}\right)}{192\bar{r}^4}+\frac{\chi\varepsilon^2De^2De_T^2\bar{p}_{,z}^3}{\bar{r}^2}\left(\frac{\beta^6\bar{R}^6}{48\bar{r}^4}-\frac{3\beta^4\bar{R}^4}{32\bar{r}^2}\right)\\&+\frac{3\chi\beta^2\varepsilon^2De^2De_T^2\bar{R}^2\bar{p}_{,z}^3}{16\bar{r}^2}+\frac{\chi\varepsilon^2De^2De_T^2\bar{p}_{,z}^3\ln(\bar{r})}{8}+\varepsilon De^2\bar{p}_{,z}^3\left(\frac{\bar{r}^4}{16}+\frac{\beta^6\bar{R}^6}{8\bar{r}^2}-\frac{3\beta^2\bar{r}^2\bar{R}^2}{8}+\frac{3\beta^4\bar{R}^4\ln(\bar{r})}{4}\right)+\frac{\chi\beta^2\varepsilon^2De_T^4\bar{R}^2\bar{p}_{,z}}{128\bar{r}^8}-\frac{\chi\varepsilon^2De_T^4\bar{p}_{,z}}{96\bar{r}^6}\\&+\frac{\beta^2\varepsilon De_T^2\bar{R}^2\bar{p}_{,z}}{16\bar{r}^4}-\frac{\varepsilon De_T^2\bar{p}_{,z}}{8\bar{r}^2}+\frac{r^2\bar{p}_{,z}}{4}-\frac{\beta^2\bar{R}^2\bar{p}_{,z}\ln(\bar{r})}{2}\end{aligned} \tag{23}$$

and

$$\begin{aligned}\bar{v}_r(\bar{r})=&-\frac{U_T}{4\bar{r}^2U}-\frac{\varepsilon De_T^2U_T}{24\bar{r}^6U}+\varepsilon De^2\left(-\frac{\beta^4\bar{R}^4U_T\bar{p}_{,z}^2}{16\bar{r}^4U}+\frac{\beta^2\bar{R}^2U_T\bar{p}_{,z}^2}{4\bar{r}^2U}+\frac{U_T\bar{p}_{,z}^2\ln(\bar{r})}{4U}\right)\\&+\frac{10U_T\chi\varepsilon^2De^4\bar{r}^4\bar{p}_{,z}^4\left(3\bar{r}^8-24\beta^2\bar{r}^6\bar{R}^2\ln(\bar{r})-18\beta^4\bar{r}^4\bar{R}^4+6\beta^6\bar{r}^2\bar{R}^6-\beta^8\bar{R}^8\right)}{960\bar{r}^{10}U}\\&+\frac{U_T\chi\left(-30\varepsilon^2De^2De_T^2\bar{r}^6\bar{p}_{,z}^2+40\beta^2\varepsilon^2De^2De_T^2\bar{r}^4\bar{R}^2\bar{p}_{,z}^2-15\beta^4\varepsilon^2De^2De_T^2\bar{r}^2\bar{R}^4\bar{p}_{,z}^2-6De_T^4\varepsilon^2\right)}{960\bar{r}^{10}U}\end{aligned} \tag{24}$$

$$\eta\frac{\mathrm{d}u}{\mathrm{d}r}=\left[1+\frac{\varepsilon\lambda}{\eta}(\tau_{zz}+\tau_{\theta\theta})+\frac{1}{2}\chi\left(\frac{\varepsilon\lambda}{\eta}(\tau_{zz}+\tau_{\theta\theta})\right)^2\right]\left[-\frac{p_{,z}\beta R}{2}\left(\frac{\beta R}{r}-\frac{r}{\beta R}\right)\right] \tag{19}$$

$$r\frac{\mathrm{d}(v/r)}{\mathrm{d}r}=\frac{M}{2\pi\eta r^2}\left[1+\frac{\varepsilon\lambda}{\eta}(\tau_{zz}+\tau_{\theta\theta})+\frac{1}{2}\chi\left(\frac{\varepsilon\lambda}{\eta}(\tau_{zz}+\tau_{\theta\theta})\right)^2\right] \tag{20}$$

Let U be the cross-section average (bulk) velocity of the annular flow, $U_T=\frac{M}{\pi\eta\zeta}$ a characteristic tangential velocity scale and $\zeta=R-\alpha R=R(1-\alpha)$ the length scale that represents the annular gap. The following dimensionless numbers can be defined: $De=\frac{\lambda U}{\zeta}$ and $De_T=\frac{\lambda U_T}{\zeta}$ which represent two Deborah numbers [19], $\bar{p}_{,z}=\frac{p_{,z}\zeta^2}{\eta U}$, $\bar{u}=\frac{u}{U}$, $\bar{v}=\frac{v}{U}$ and $\bar{r}=\frac{r}{\zeta}$. After substituting the stress components by the expressions of Eqs. 17, Eq. 20 can be rewritten in dimensionless form as,

$$\begin{aligned}\frac{\mathrm{d}\bar{u}}{\mathrm{d}\bar{r}}=&\left\{1+2\varepsilon De^2\left[\frac{\bar{p}_{,z}\beta\bar{R}}{2}\left(\frac{\beta\bar{R}}{\bar{r}}-\frac{\bar{r}}{\beta\bar{R}}\right)\right]^2+\frac{\varepsilon De_T^2}{2\bar{r}^4}\right.\\&\left.+\frac{1}{2}\chi\left(2\varepsilon De^2\left[\frac{\bar{p}_{,z}\beta\bar{R}}{2}\left(\frac{\beta\bar{R}}{\bar{r}}-\frac{\bar{r}}{\beta\bar{R}}\right)\right]^2+\frac{\varepsilon De_T^2}{2\bar{r}^4}\right)^2\right\}\\&\times\left[-\frac{\bar{p}_{,z}\beta\bar{R}}{2}\left(\frac{\beta\bar{R}}{\bar{r}}-\frac{\bar{r}}{\beta\bar{R}}\right)\right]\end{aligned} \tag{21}$$

where $\bar{c}_b$ and $\bar{c}_c$ are dimensionless integration constants.

3.1.1. Axial flow

The axial boundary conditions at the inner and outer cylinder allow the determination of constants $\bar{c}_c$ and β. Based on Fig. 2 we can see that the boundary condition for the slip velocity at the inner cylinder is given by $u(\alpha R)=k_i|\tau_{rz}|^{m_i-1}\tau_{rz}$ [3,4] and at the outer cylinder by $u(R)=-k_o|\tau_{rz}|^{m_o-1}\tau_{rz}$, with k and m representing, respectively, the slip law coefficient and exponent that can have different intensities at the inner and outer walls (subscripts i and o stand for "inner" and "outer"). These boundary conditions can be written in dimensionless form as,

$$\bar{u}(\alpha\bar{R})=\bar{k}_i\left[-\bar{p}_{,z}\frac{\beta\bar{R}}{2}\left(\frac{\beta}{\alpha}-\frac{\alpha}{\beta}\right)\right]^{m_i} \tag{25}$$

$$\bar{u}(\bar{R})=\bar{k}_o\left[\bar{p}_{,z}\frac{\beta\bar{R}}{2}\left(\beta-\frac{1}{\beta}\right)\right]^{m_o} \tag{26}$$

where $\bar{k}_i=\left(\frac{k_i\eta}{\zeta}\right)\left(\frac{|U|\eta}{\zeta}\right)^{m_i-1}$ and $\bar{k}_o=\left(\frac{k_o\eta}{\zeta}\right)\left(\frac{|U|\eta}{\zeta}\right)^{m_o-1}$.

Using Eq. (25) in $\bar{u}(\bar{r})=\bar{u}_a(\bar{r})+\bar{c}_b$, together with the velocity profile of Eq. (23) determines $\bar{c}_b$ and further manipulation gives,

$$\bar{u}(\bar{r})=\bar{u}_a(\bar{r})-\bar{u}_a(\alpha\bar{R})+\bar{k}_i\left[-\bar{p}_{,z}\frac{\beta\bar{R}}{2}\left(\frac{\beta}{\alpha}-\frac{\alpha}{\beta}\right)\right]^{m_i}. \tag{27}$$

Then, substituting Eq. (26) in Eq. (27) leads to the following equation for β,

$$f_1\left(\frac{U_T}{U},\bar{p}_{,z},\beta\right)\equiv \bar{u}_a(\overline{R})-\bar{u}_a(\alpha\overline{R})+\bar{k}_i\left[-\bar{p}_{,z}\frac{\beta\overline{R}}{2}\left(\frac{\beta}{\alpha}-\frac{\alpha}{\beta}\right)\right]^{m_i} - \bar{k}_o\left[\bar{p}_{,z}\frac{\beta\overline{R}}{2}\left(\beta-\frac{1}{\beta}\right)\right]^{m_o}=0 \tag{28}$$

$\chi=0$ (linear PTT), an explicit analytical solution can be obtained for the cases ($m=m_i=m_o$) $m=1$ (linear Navier slip law), $m=2$, $m=3$, given by,

$$\begin{aligned}
\beta &= [A+B]^{\frac{1}{2}}\\
A &= \frac{\sqrt[3]{-2a_2^3+9a_1a_3a_2-27a_0a_3^2+\sqrt{4\left(3a_1a_3-a_2^2\right)^3+\left(-2a_2^3+9a_1a_3a_2-27a_0a_3^2\right)^2}}}{3\sqrt[3]{2}a_3}\\
B &= -\frac{a_2}{3a_3}-\frac{\sqrt[3]{2}\left(3a_1a_3-a_2^2\right)}{3a_3\sqrt[3]{-2a_2^3+9a_1a_3a_2-27a_0a_3^2+\sqrt{4\left(3a_1a_3-a_2^2\right)^3+\left(-2a_2^3+9a_1a_3a_2-27a_0a_3^2\right)^2}}}
\end{aligned} \tag{29}$$

with

$$\begin{aligned}
a_0 &= -\frac{\overline{R}\bar{p}_{,z}\left((\alpha^2-1)\alpha^2\varepsilon De^2\overline{R}^3\bar{p}_{,z}^2+(\alpha^2-1)\alpha^4\varepsilon De^2\overline{R}^3\bar{p}_{,z}^2-8\alpha^3\bar{k}_i-8\alpha^2\bar{k}_0+4\alpha^4\overline{R}-4\alpha^2\overline{R}\right)}{16\alpha^2}\\
a_1 &= -\frac{\overline{R}\bar{p}_{,z}\left(-6\alpha^2(\alpha^2-1)\varepsilon De^2\overline{R}^3\bar{p}_{,z}^2+8\alpha\bar{k}_i+8\alpha^2\bar{k}_0+8\alpha^2\overline{R}\ln(\overline{R})-8\alpha^2\overline{R}\ln(\alpha\overline{R})\right)}{16\alpha^2}\\
a_2 &= -\frac{\overline{R}\bar{p}_{,z}\left(12\alpha^2\varepsilon De^2\overline{R}^3\bar{p}_{,z}^2\ln(\alpha\overline{R})-12\alpha^2De^2\varepsilon\overline{R}^3\bar{p}_{,z}^2\ln(\overline{R})\right)}{16\alpha^2}\\
a_3 &= \frac{(\alpha^2-1)De^2\varepsilon\overline{R}^4\bar{p}_{,z}^3}{8\alpha^2}
\end{aligned} \tag{30}$$

for $m=1$,

$$\begin{aligned}
a_0 &= \frac{\overline{R}^2\bar{p}_{,z}\left(-4\alpha^4+4\alpha^2+\alpha^6\left(-\varepsilon De^2\right)\overline{R}^2\bar{p}_{,z}^2+\alpha^2\varepsilon De^2\overline{R}^2\bar{p}_{,z}^2+4\alpha^4\bar{k}_i\bar{p}_{,z}-4\alpha^2\bar{k}_0\bar{p}_{,z}\right)}{16\alpha^2}\\
a_1 &= \frac{\overline{R}^2\bar{p}_{,z}\left(6\alpha^4\varepsilon De^2\overline{R}^2\bar{p}_{,z}^2-6\alpha^2\varepsilon De^2\overline{R}^2\bar{p}_{,z}^2-8\alpha^2\bar{k}_i\bar{p}_{,z}+8\alpha^2\bar{k}_0\bar{p}_{,z}-8\alpha^2\ln(\overline{R})+8\alpha^2\ln(\alpha\overline{R})\right)}{16\alpha^2}\\
a_2 &= \frac{\overline{R}^2\bar{p}_{,z}\left(12\alpha^2\varepsilon De^2\overline{R}^2\bar{p}_{,z}^2\ln(\overline{R})-12\alpha^2De^2\varepsilon\overline{R}^2\bar{p}_{,z}^2\ln(\alpha\overline{R})+4\bar{k}_i\bar{p}_{,z}-4\alpha^2\bar{k}_0\bar{p}_{,z}\right)}{16\alpha^2}\\
a_3 &= \frac{\overline{R}^2\bar{p}_{,z}\left(2\alpha^2\varepsilon De^2\overline{R}^2\bar{p}_{,z}^2-2De^2\varepsilon\overline{R}^2\bar{p}_{,z}^2\right)}{16\alpha^2}
\end{aligned} \tag{31}$$

for $m=2$, and

$$\begin{aligned}
a_0 &= \frac{\overline{R}^2\bar{p}_{,z}\left(-4\alpha^5+4\alpha^3+(1-\alpha^2)\alpha^5\varepsilon De^2\overline{R}^2\bar{p}_{,z}^2+(1-\alpha^2)\alpha^3\varepsilon De^2\overline{R}^2\bar{p}_{,z}^2+2\alpha^6\overline{R}\bar{k}_i\bar{p}_{,z}^2+2\alpha^3\bar{k}_0\overline{R}\bar{p}_{,z}^2\right)}{16\alpha^3}\\
a_1 &= \frac{\overline{R}^2\bar{p}_{,z}\left(-6(1-\alpha^2)\alpha^3\varepsilon De^2\overline{R}^2\bar{p}_{,z}^2-6\alpha^4\overline{R}\bar{k}_i\bar{p}_{,z}^2-6\alpha^3\bar{k}_0\overline{R}\bar{p}_{,z}^2-8\alpha^3\ln(\overline{R})+8\alpha^3\ln(\alpha\overline{R})\right)}{16\alpha^3}\\
a_2 &= \frac{\overline{R}^2\bar{p}_{,z}\left(12\alpha^3\varepsilon De^2\overline{R}^2\bar{p}_{,z}^2\ln(\overline{R})-12\alpha^3\varepsilon De^2\overline{R}^2\bar{p}_{,z}^2\ln(\alpha\overline{R})+6\alpha^2\overline{R}\bar{k}_i\bar{p}_{,z}^2+6\alpha^3\bar{k}_0\overline{R}\bar{p}_{,z}^2\right)}{16\alpha^3}\\
a_3 &= \frac{\overline{R}^2\bar{p}_{,z}\left(-2(1-\alpha^2)\alpha\varepsilon De^2\overline{R}^2\bar{p}_{,z}^2-2\overline{R}\bar{k}_i\bar{p}_{,z}^2-2\alpha^3\bar{k}_0\overline{R}\bar{p}_{,z}^2\right)}{16\alpha^3}
\end{aligned} \tag{32}$$

Note that $\alpha<\beta<1$ and that this equation depends also on the dimensionless pressure gradient $\bar{p}_{,z}$ (a negative parameter) and the torque M. This is a transcendental equation for most of the exponents m but it can be easily solved by numerical methods such as fixed point iteration methods.

The analytical solutions for the linear PTT model with no slip boundary conditions ($k_i=k_o=0$) were presented elsewhere [18], but the analytical solution for the linear PTT model with slip velocity and quadratic PTT model with and without slip velocity could not be found in the literature. Assuming pure axial flow and for $m=3$. More details are presented in Appendix A.

By imposing a mean axial velocity U, another equation emerges that will be helpful for the solution of the direct problem (U and ω are given and we want to determine the pressure drop, $\bar{p}_{,z}$, and the torque, M).

To determine the pressure gradient for a given flow rate the following equation must be solved,

$$U=\frac{1}{\pi R^2(1-\alpha^2)}\int_{\alpha R}^{R}u(r)2\pi r\,\mathrm{d}r \tag{33}$$

where $\pi R^2(1-\alpha^2)$ is the area of the cross section of the annular region. Based on the definition $\bar{r}=\frac{r}{\zeta}$ and $\mathrm{d}r=\zeta\,\mathrm{d}\bar{r}$, the dimensionless equation to be solved is,

$$\frac{2}{\overline{R}^2(1-\alpha^2)}\int_{\alpha\overline{R}}^{\overline{R}}\bar{u}(\bar{r})\bar{r}\mathrm{d}\bar{r}-1=0 \tag{34}$$

with $\bar{u}(\bar{r})$ given by Eq. (27). Upon integration we obtain the following transcendental equation for $\bar{p}_{,z}$,

$$f_2\left(\frac{U_T}{U},\bar{p}_{,z},\beta\right)\equiv\chi d_1\bar{p}_{,z}^5+d_2\bar{p}_{,z}^3+d_3\bar{p}_{,z}+d_4(-\bar{p}_{,z})^{m_i}-(1-\alpha^2)=0 \tag{35}$$

where

$$\begin{aligned}
d_1=&\varepsilon^2De^4\left(\frac{\overline{R}^6}{384}-\frac{\alpha^6\overline{R}^6}{96}+\frac{\alpha^8\overline{R}^6}{128}-\frac{5\beta^2\overline{R}^6}{192}+\frac{5\alpha^4\beta^2\overline{R}^6}{64}\right.\\
&\left.-\frac{5\alpha^6\beta^2\overline{R}^6}{96}+\frac{5\beta^4\overline{R}^6}{32}-\frac{5\alpha^2\beta^4\overline{R}^6}{16}\right)+\varepsilon^2De^4\left(\frac{5\alpha^4\beta^4\overline{R}^6}{32}+\frac{5\beta^6\overline{R}^6}{16}\right.\\
&\left.-\frac{5\alpha^2\beta^6\overline{R}^6}{16}-\frac{5\beta^8\overline{R}^6}{32}+\frac{5\beta^8\overline{R}^6}{32\alpha^2}-\frac{\beta^{10}\overline{R}^6}{64}-\frac{\beta^{10}\overline{R}^6}{64\alpha^4}+\frac{\beta^{10}\overline{R}^6}{32\alpha^2}\right)\\
&+\varepsilon^2De^4\overline{R}^6\ln(\alpha)\left(\frac{5\beta^8}{16}+\frac{5\beta^6}{8}\right)\\
d_2=&\varepsilon De^2\left(\frac{\overline{R}^4}{48}-\frac{\alpha^4\overline{R}^4}{16}+\frac{\alpha^6\overline{R}^4}{24}-\frac{3\beta^2\overline{R}^4}{16}+\frac{3\alpha^2\beta^2\overline{R}^4}{8}-\frac{3\alpha^4\beta^2\overline{R}^4}{16}\right.\\
&\left.-\frac{3\beta^4\overline{R}^4}{8}+\frac{3\alpha^2\beta^4\overline{R}^4}{8}+\frac{\beta^6\overline{R}^4}{8}-\frac{\beta^6\overline{R}^4}{8\alpha^2}\right)+\varepsilon De^2\overline{R}^4\ln(\alpha)\left(-\frac{\beta^6}{4}-\frac{3\beta^4}{4}\right)\\
&+\varepsilon^2De^2De_T^2\chi\left(\frac{3\beta^2}{16}-\frac{3\beta^2}{16\alpha^2}+\frac{3\beta^4}{32}+\frac{3\beta^4}{32\alpha^4}-\frac{3\beta^4}{16\alpha^2}-\frac{\beta^6}{96}\right.\\
&\left.-\frac{\beta^6}{48\alpha^6}+\frac{\beta^6}{32\alpha^4}\right)+\varepsilon^2De^2De_T^2\chi\left(-\frac{3\beta^2\ln(\alpha)}{8}-\frac{\ln(\alpha)}{8}-\frac{1}{16}+\frac{\alpha^2}{16}\right)\\
d_3=&\frac{\overline{R}^2}{8}-\frac{\alpha^2\overline{R}^2}{4}+\frac{\alpha^4\overline{R}^2}{8}+\frac{\beta^2\overline{R}^2}{4}-\frac{\alpha^2\beta^2\overline{R}^2}{4}+\varepsilon De_T^2\left(-\frac{1}{8\overline{R}^2}+\frac{1}{8\alpha^2\overline{R}^2}\right.\\
&\left.-\frac{\beta^2}{16\overline{R}^2}-\frac{\beta^2}{16\alpha^4\overline{R}^2}+\frac{\beta^2}{8\alpha^2\overline{R}^2}\right)+\varepsilon^2De_T^4\chi\left(-\frac{\beta^2}{128\alpha^8\overline{R}^6}+\frac{\beta^2}{96\alpha^6\overline{R}^6}\right.\\
&\left.+\frac{1}{96\alpha^6\overline{R}^6}-\frac{1}{64\alpha^4\overline{R}^6}-\frac{\beta^2}{384\overline{R}^6}+\frac{1}{192\overline{R}^6}\right)+\frac{\varepsilon De_T^2\ln(\alpha)}{4\overline{R}^2}+\frac{\beta^2\overline{R}^2\ln(\alpha)}{2}\\
d_4=&\bar{k}_i\left[\frac{(\beta^2-\alpha^2)\overline{R}}{2\alpha}\right]^{m_i}(1-\alpha^2)
\end{aligned} \tag{36}$$

3.1.2. Azimuthal flow

Once β is known, Eq. (24) is only missing the value of the integration constant $\bar{c}_c$ for the solution to be complete. For that we still have two transverse slip boundary conditions that are given for the inner cylinder by $v(\alpha R)=\omega\alpha R+k_{vi}\|\tau_{r\theta}\|^{m_{vi}-1}\tau_{r\theta}$ (difference between the wall velocity ($\omega\alpha R$) and the slip velocity) and for the outer cylinder by $v(R)=-k_{vo}\|\tau_{r\theta}\|^{m_{vo}-1}\tau_{r\theta}$ (Fig. 2). The boundary conditions can be written in dimensionless form as,

$$\bar{v}(\alpha\overline{R})=\overline{\omega}\alpha\overline{R}+\bar{k}_{vi}\frac{\left|\frac{U_T}{U}\right|^{m_{vi}-1}\left(\frac{U_T}{U}\right)}{(\alpha\overline{R})^{2m_{vi}}} \tag{37}$$

$$\bar{v}(\overline{R})=-\bar{k}_{vo}\frac{\left|\frac{U_T}{U}\right|^{m_{vo}-1}\left(\frac{U_T}{U}\right)}{(\overline{R})^{2m_{vo}}} \tag{38}$$

where $\bar{k}_{vi}=\frac{k_{vi}}{|U|}\left(\frac{\eta|U|}{2\zeta}\right)^{m_{vi}}$, $\bar{k}_{vo}=\frac{k_{vo}}{|U|}\left(\frac{\eta|U|}{2\zeta}\right)^{m_{vo}}$ and $\overline{\omega}=\frac{\omega\zeta}{U}$ (note that the slip coefficients for the tangential slip velocity (Eqs. (37) and (38)) can be, in general, different from the ones used in the axial slip velocity (Eqs. (25) and (26)).

With the help of Eq. (38) and with $\bar{v}(\bar{r})=\bar{r}\bar{v}_r(\bar{r})+\bar{c}_c\bar{r}$ the integration constant $\bar{c}_c$ can be determined and the tangential velocity profile is given by,

$$\bar{v}(\bar{r})=\bar{r}\bar{v}_r(\bar{r})-\bar{r}\bar{v}_r(\overline{R})-\bar{k}_{vo}\frac{\left|\frac{U_T}{U}\right|^{m_{vo}-1}\left(\frac{U_T}{U}\right)}{(\overline{R})^{2m_{vo}}}\frac{\bar{r}}{\overline{R}} \tag{39}$$

Substituting Eq. (37) into Eq. (39) leads to the following equation for U_T,

$$\begin{aligned}
f_3\left(\frac{U_T}{U},\bar{p}_{,z},\beta\right)\equiv&\,\bar{v}_r(\alpha\overline{R})\alpha\overline{R}-\bar{v}_r(\overline{R})\alpha\overline{R}-\bar{k}_{vo}\frac{\left|\frac{U_T}{U}\right|^{m_{vo}-1}\left(\frac{U_T}{U}\right)}{(\overline{R})^{2m_{vo}}}\alpha\\
&-\left[\overline{\omega}\alpha\overline{R}+\bar{k}_{vi}\frac{\left|\frac{U_T}{U}\right|^{m_{vi}-1}\left(\frac{U_T}{U}\right)}{(\alpha\overline{R})^{2m_{vi}}}\right]=0
\end{aligned} \tag{40}$$

3.1.3. Solution method

Two different types of solution methods can be used for the direct and the inverse problems. For the direct solution, U and ω are given and we need to determine M (via U_T), $\bar{p}_{,z},\beta$. In order to do that, the following nonlinear system of equations must be solved,

$$\begin{cases}f_1\left(\frac{U_T}{U},\bar{p}_{,z},\beta\right)=0\\ f_2\left(\frac{U_T}{U},\bar{p}_{,z},\beta\right)=0\\ f_3\left(\frac{U_T}{U},\bar{p}_{,z},\beta\right)=0\end{cases} \tag{41}$$

For the inverse problem, M and $p_{,z}$ are given, and we can easily obtain β,U and ω with the same previous system of equations.

3.2. Exponential PTT model (pure axial flow)

For the pure axial flow of a fluid modeled by the exponential PTT model, it is still possible to use a simple numerical method for the pure axial flow problem.

The dimensionless velocity gradient for the exponential PTT model is given by,

$$\begin{aligned}
\frac{\mathrm{d}\bar{u}}{\mathrm{d}\bar{r}}=&\left[-\frac{\bar{p}_{,z}\beta\overline{R}}{2}\left(\frac{\beta\overline{R}}{\bar{r}}-\frac{\bar{r}}{\beta\overline{R}}\right)\right]\exp\left\{2\varepsilon De^2\left[\frac{\bar{p}_{,z}\beta\overline{R}}{2}\left(\frac{\beta\overline{R}}{\bar{r}}-\frac{\bar{r}}{\beta\overline{R}}\right)\right]^2+\frac{\varepsilon De_T^2}{2\bar{r}^4}\right\}\\
\equiv&f(\bar{r})
\end{aligned} \tag{42}$$

Upon integration and using the slip boundary condition $\bar{u}(\alpha\overline{R})$ at the inner cylinder from Eq. (25), we obtain,

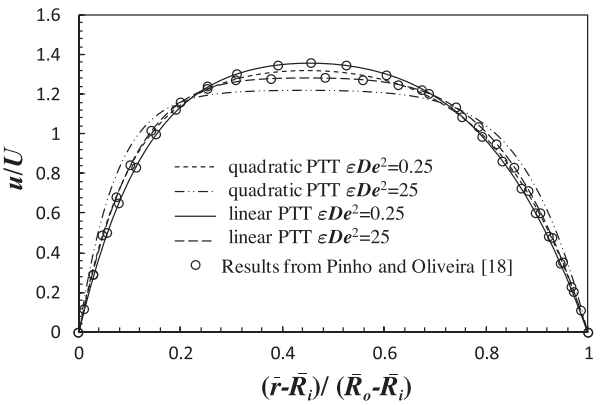

Fig. 3. Velocity profiles for the linear and quadratic PTT models with $\varepsilon De^2=0.25$ and 25, $\alpha=0.5$ and $\bar{k}_i=\bar{k}_o=0$.

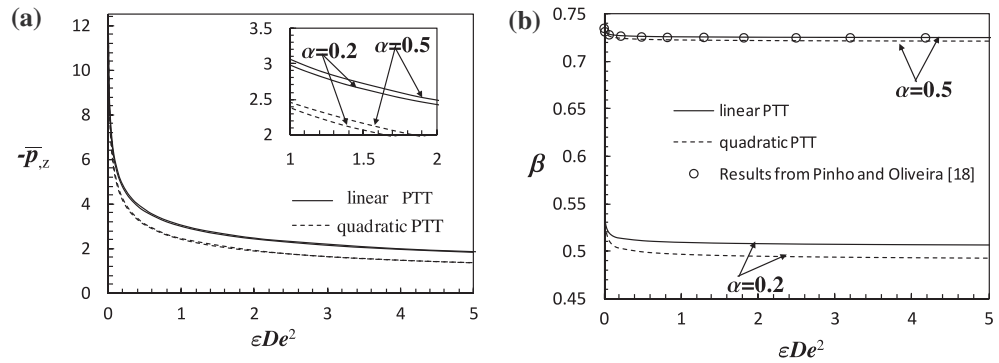

Fig. 4. Variation of the dimensionless pressure drop, $\bar{p}_{,z}$, (a) and β (b) with εDe^2, for the no-slip case ($\bar{k}_i = \bar{k}_o = 0$) and two different cylinder ratios $\alpha = 0.2$ and 0.5.

$$\bar{u}(\bar{r}) = \int_{\alpha\bar{R}}^{\bar{r}} f(\bar{r})\mathrm{d}\bar{r} + \bar{k}_i\left[-\bar{p}_{,z}\frac{\beta\bar{R}}{2}\left(\frac{\beta}{\alpha}-\frac{\alpha}{\beta}\right)\right]^{m_i} \tag{43}$$

With the help of the slip boundary condition at the outer cylinder, Eq. (26), we can obtain β by solving,

$$\int_{\alpha\bar{R}}^{\bar{R}} f(\bar{r})\mathrm{d}\bar{r} + \bar{k}_i\left[-\bar{p}_{,z}\frac{\beta\bar{R}}{2}\left(\frac{\beta}{\alpha}-\frac{\alpha}{\beta}\right)\right]^{m_i} - \bar{k}_o\left[\bar{p}_{,z}\frac{\beta\bar{R}}{2}\left(\beta-\frac{1}{\beta}\right)\right]^{m_o} = 0 \tag{44}$$

The numerical procedure to obtain the velocity profile involves the solution of Eq. (44) for β (note that Eq. (43) written in dimensional form is independent of U). With the value of β we obtain function $f(\bar{r})$, and Eq. (43) can now be numerically integrated for each $\bar{r}$ in the range $\alpha\bar{R} < \bar{r} < \bar{R}$, and used to solve the nonlinear Eq. (34) for the inverse flow problem. For the numerical integration of Eq. (43) we used the Simpson's 1/3 rule, and for the numerical solution of Eq. (44) we used the bisection method for β in the range $]\alpha, 1[$.

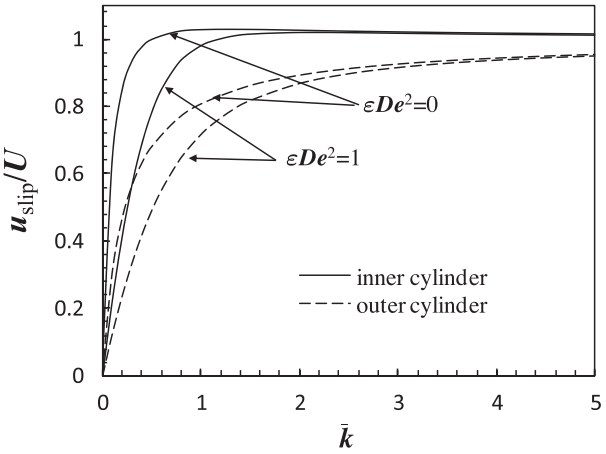

Fig. 6. Variation of the linear ($m = 1$) wall slip velocity at the inner (Eq. (25)) and outer (Eq. (26)) cylinders for $\bar{k} = \bar{k}_i = \bar{k}_o$, $\alpha = 0.1$ and considering $\varepsilon De^2 = 0$ and 1.

4. Results

The equations derived in the previous section will now be analyzed in terms of velocity and extra-stress profiles with and without the occurrence of wall slip velocity. Because similar case studies have been extensively investigated for the linear PTT model without slip velocity [18,19], we will focus on the differences between the viscoelastic models and on the effects of the slip coefficient on the velocity profiles. First we will study the pure axial flow and then we will study the helical flow for the linear and quadratic PTT models.

To quantify the combination of axial and rotational flow we use the Reynolds and Taylor numbers, respectively, here defined as,

$$Re = \frac{2\zeta\rho U}{\eta} \tag{45}$$

$$Ta = \left(\frac{1}{\alpha}-1\right)\left(\frac{Re}{2De}\right)^2 De_{Ti}^2 \tag{46}$$

where $De_{Ti} = \frac{\lambda\omega\alpha R}{\zeta}$ is a Deborah number related to the rotation of the inner cylinder [5,19].

4.1. Linear and quadratic PTT models

4.1.1. Pure axial flow with no-slip

Fig. 3 shows velocity profiles for the linear and quadratic viscoelastic models assuming no-slip conditions at both walls. It can be seen that the quadratic model shows a more pronounced plug flow velocity profile when compared to the linear model, an evidence of a stronger shear thinning, in agreement with Fig. 1. These results were compared with data existing in the literature for the linear PTT model, and, as expected, our results match exactly the ones from Pinho and Oliveira [18].

To present a more detailed comparison between the linear and quadratic PTT models, Fig. 4 shows the variation of the normalized

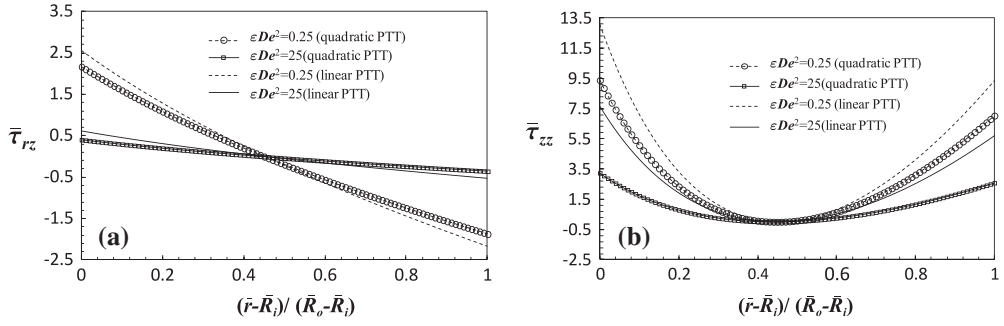

Fig. 5. Normalized stress profiles ($\bar{\tau}_{ij} = \tau_{ij}/(\eta U/\zeta)$) of the linear and quadratic PTT models with $\alpha = 0.5$, and $\varepsilon De^2 = 0.25$ and 25 (a) $\bar{\tau}_{rz}$ (b) $\bar{\tau}_{zz}$.

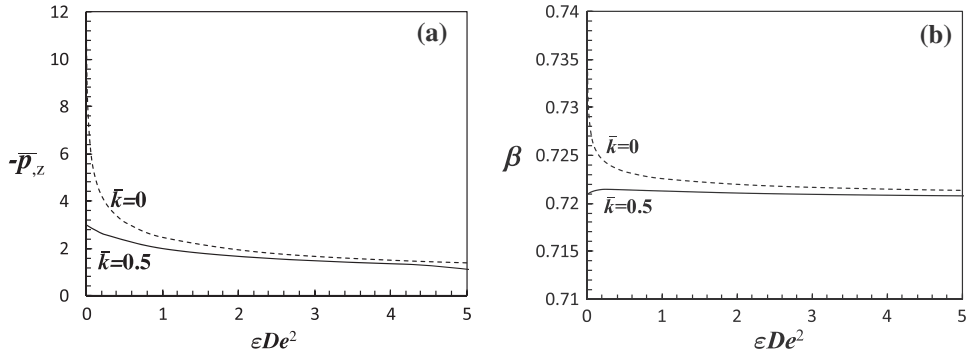

Fig. 7. Variation of dimensionless pressure drop, $\bar{p}_{,z}$, (a) and β (b) with εDe^2, for the quadratic PTT model with $\alpha = 0.5,\ m = 1$ and $\bar{k}_i = \bar{k}_o = 0$ and 0.5.

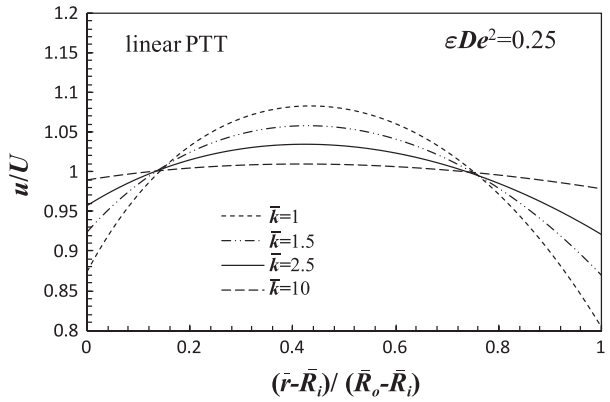

Fig. 8. Velocity profiles for the linear PTT model with $\alpha = 0.5,\ \varepsilon De^2 = 0.25$, and four different values of the slip coefficients, $\bar{k} = \bar{k}_i = \bar{k}_o = 1, 1.5, 2.5, 10$, for the linear slip model, $m = 1$.

pressure gradient, and of β, both as function of εDe^2. Both quantities decrease for decreasing cylinder ratio, with smaller values obtained for the quadratic model. This means that for higher εDe^2 one needs a smaller pressure drop to obtain the same flow rate, due to increasing shear thinning of the quadratic PTT model relative to the linear PTT model. Note also that the location of the zero shear stress β moves towards the inner cylinder with the increase of εDe^2. As shown in [35], for the flow between parallel plates, the reduction of the wall resistance in only one of the walls, leads to the breakup of symmetry, with the maximum velocity approaching the less restrictive wall. For the annular flow, although the wall shear stress is locally smaller at the outer cylinder, the fact that the outer cylinder has a larger radius promotes an higher total shear force at the cylinder surface. This justifies the fact that β approaches the inner cylinder. As εDe^2 increases, the viscosity decreases, increasing the fluidity of the flow, especially near the inner cylinder since it is a region of higher shear rates, forcing β to move further in the radial location of the inner cylinder direction.

The radial profiles of the extra-stress for the quadratic and linear models were also investigated (Fig. 5(a) and (b)) for the case with no slip at the walls and for different values of εDe^2. For both models the dimensionless normal stress is always positive and the dimensionless shear stress shows a quasi-linear profile, being positive near the inner cylinder and negative in the vicinity of the outer cylinder. For constant flow rate, the quadratic model shows smaller dimensionless extra-stress values when compared to the linear model since the quadratic model has lower Ψ_1 values than the linear model, as shown in Fig. 1.

4.1.2. Pure axial flow with slip at the walls

In order to understand the influence of wall slip velocity on the velocity and stress profiles, we first analyze in detail the slip velocity models given by Eqs. (25) and (26). The idea is to show how the slip velocities $\bar{u}(\alpha\bar{R})$ and $\bar{u}(\bar{R})$ behave with the variation of $\bar{k}$.

In Fig. 6 we show the variation of the slip velocity with the slip coefficient for $\alpha = 0.1$ and considering $\varepsilon De^2 = 0$ and 1. As expected, even for the case $\bar{k}_i = \bar{k}_o$ different slip velocities are obtained, in contrast with the Poiseuille flow between parallel plates, because the stresses at the inner and outer walls are different due to their different curvatures (as shown before for the no-slip case). A simple analysis shows that the same slip velocity at the inner and outer walls is obtained when $\beta = \sqrt{\alpha}$ and $\bar{k}_i = \bar{k}_o$. This is why the slip velocities at the inner and outer cylinders are similar for large slip coefficients.

The influence of slip velocity on the behavior of $-\bar{p}_{,z}$ and β was also studied. We show in Fig. 7(a) and (b) the variation of $-\bar{p}_{,z}$ and

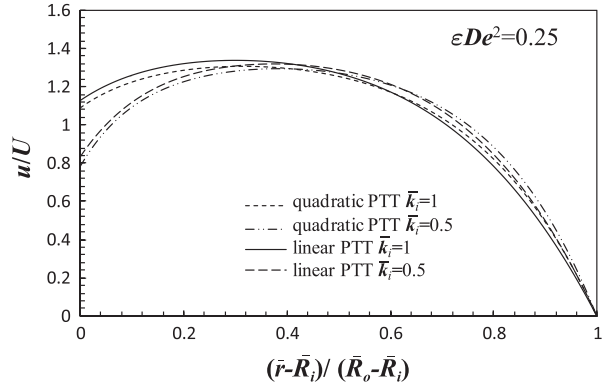

Fig. 9. Velocity profiles for the linear and quadratic PTT models with $\varepsilon De^2 = 0.25,\ \alpha = 0.5,\ m = 1,\ \bar{k}_i = 0.5$ and 1, and $\bar{k}_o = 0$.

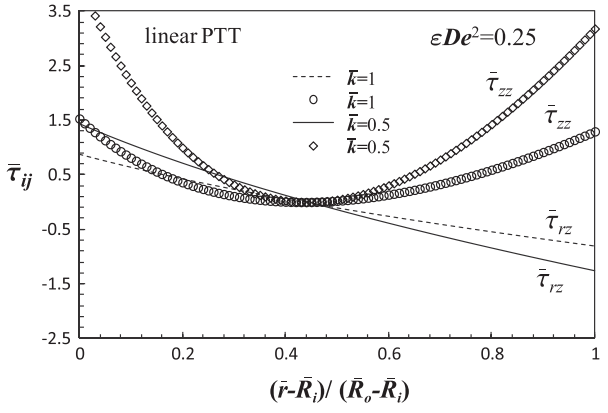

Fig. 10. Stress profiles for the linear PTT model for $\varepsilon De^2 = 0.25,\ \alpha = 0.5,\ m = 1$, and $\bar{k} = 0.5$ and 1.

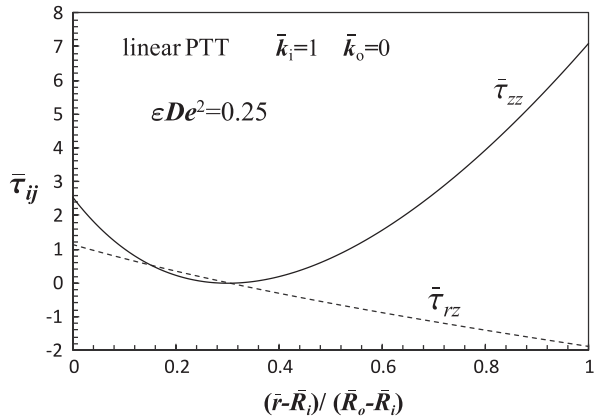

Fig. 11. Stress profiles for the linear PTT model with slip velocity at the inner cylinder. ($\bar{k}_i = 1,\ \bar{k}_o = 0,\ \alpha = 0.5,\ m = 1$ and $\varepsilon De^2 = 0.25$).

β with εDe^2 for the no slip case and for $\bar{k}_i = \bar{k}_o = 0.5$. Since wall friction decreases when wall slip increases, both the pressure drop and β decrease regardless of εDe^2 for $\bar{k} = 0.5$. In the same lines of thought given before for the no-slip case, in the presence of slip velocity, β decreases because the large shear stresses at the inner wall result in higher slip velocities, so the location of the maximum velocity approaches the inner wall.

In Fig. 8 we illustrate the consequences of wall slip on the shape of the velocity profile. Using the linear PTT model and the same slip coefficient at both cylinders, we show that the inner cylinder always has a higher slip velocity (because of the higher stresses), but as the friction coefficients increase the differences in slip between the two walls tend to decrease. This happens because we approach a plug velocity profile, and for very high slip coefficients the slip velocity at the both walls approaches the bulk velocity. Note that when $\bar{k} \to \infty$ a perfect plug profile would be obtained. For this case the position of the maximum velocity is undetermined, but, as the previous results suggest, the curvature of the velocity profile would degenerate into a constant velocity profile with the maximum velocity position converging to the plug profile from a position near the inner cylinder.

In Fig. 9 we present velocity profiles with slip velocity only at the inner cylinder, illustrating that the quadratic model shows a smaller slip velocity and that the shape of the velocity profile approaches a half parabola with the increase of the slip coefficient. This also shows that β moves towards the radial position of the inner cylinder wall that possesses higher slip velocity.

The stress radial profiles were also studied for the case of slip velocity (Figs. 10 and 11). As expected, increasing the slip velocity coefficient leads to velocity profiles approaching a plug shape and the normalized extra-stress components decrease (see Fig. 10). When a high slip velocity coefficient is applied only at the inner cylinder, the extra-stress components tend to zero at the wall where the fluid slips (Fig. 11). The same happens with the outer wall, although this is not shown here for conciseness.

4.1.3. Helical flow

Pure axial and helical flows are qualitative different types of flows (pressure driven axial flow versus Couette rotational flow): whereas the axial flow is forced by a pressure gradient and shear stresses are a resisting force, in tangential flow the driving mechanism is the shear stress dragging the neighbor fluid, but the shear stress on the outer wall acts as a resistance force. Hence, the stronger shear thinning of the quadratic model inevitably increases the near-wall velocities in axial flow, but reduces the near wall velocities in tangential flow, when compared with the less shear-thinning linear PTT fluid.

To study the helical flow it is instructive to analyze the effect of the velocity ratio, $\frac{\omega\alpha R}{U}$. According to Escudier et al. [6] and Cruz and Pinho [19], for $\frac{\omega\alpha R}{U} < 1$ an axial dominated flow is observed, while and for $\frac{\omega\alpha R}{U} > 10$ the rotational flow is dominant.

In Fig. 12(a) and (b) we plot the axial and tangential velocity profiles for the linear and quadratic viscoelastic models at constant $\varepsilon De^2 = 0.25$ and $\frac{\omega\alpha R}{U} = 0.1$. For u, the linear model shows higher maximum velocity when compared with the quadratic model (due to the shear thinning effect, the velocity profile for the quadratic model is blunter). In the presence of wall slip the differences between the two models are reduced, as both models show similar velocity profiles with the rotational flow tending to a plug as slip increases.

When the rotational flow is dominant (Fig. 13(a) and (b)) the differences between the two models are enhanced. The quadratic model shows a smaller β, meaning that the maximum axial velocity u occurs near the inner cylinder because there is a larger reduction of the axial shear stress for the quadratic PTT model, when there is slip in a rotational-dominant flow (note that the same happened with the pure axial flow, as shown in Figs. 10 and 11). Also note that for the axial dominant flow, higher slip velocities are obtained for the same slip coefficients than in rotational-dominant flows.

In order to better understand the behavior of these different types of flow under wall slip boundary conditions we also plot the velocity profiles for the linear PTT model assuming different slip boundary conditions at the wall (Fig. 14(a) and (b)). We assume no-slip at the inner cylinder, while the outer cylinder is made of a slippery surface. As we increase the slip coefficient, Fig. 14(b) shows that the inner cylinder rotation is dragging the fluid around the annulus with an enhanced transport of momentum across the

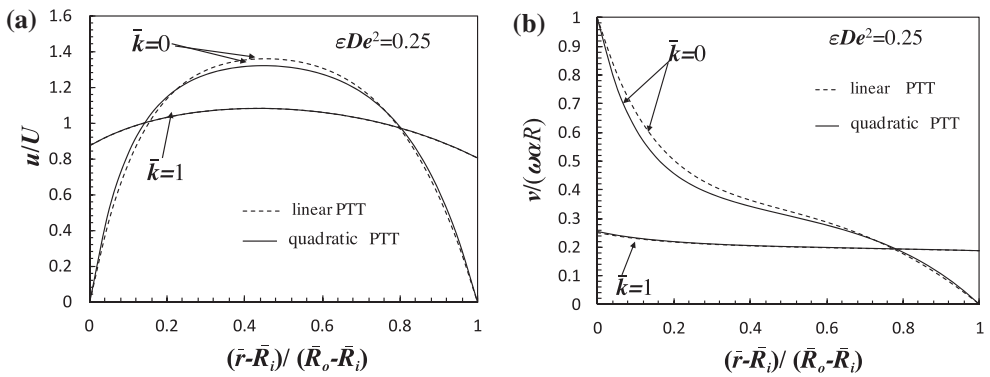

Fig. 12. Velocity profiles for axial dominant flow ($\frac{\omega\alpha R}{U} = 0.1$) of the linear and quadratic PTT models with $\alpha = 0.5,\ \varepsilon De^2 = 0.25$ and two different values of the slip coefficient, $\bar{k} = \bar{k}_i = \bar{k}_0 = 0$ and 1 ($Re = 1000,\ Ta = 2500$).

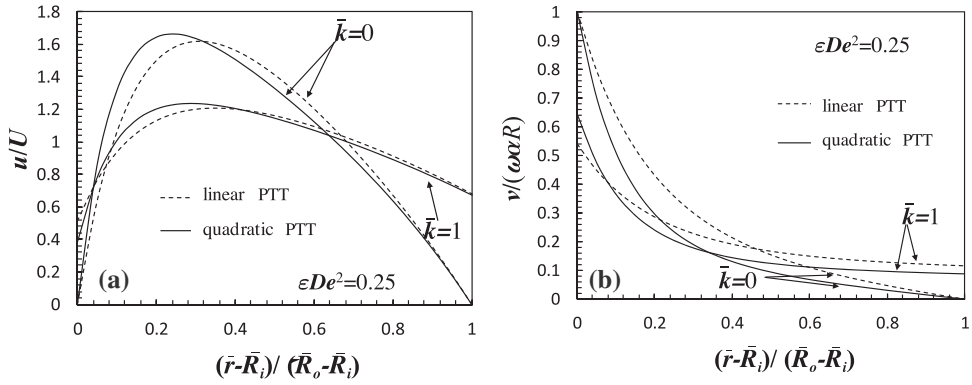

Fig. 13. Velocity profiles for the rotational dominant flow $\left(\frac{\omega\alpha R}{U}=20\right)$ of the linear and quadratic PTT models with $\alpha=0.5,\ \varepsilon De^2=0.25$ and two different values of the slip coefficient, $\bar{k}=\bar{k}_i=\bar{k}_0=0$ and 1 $\left(Re=10^3,\ Ta=10^8\right)$.

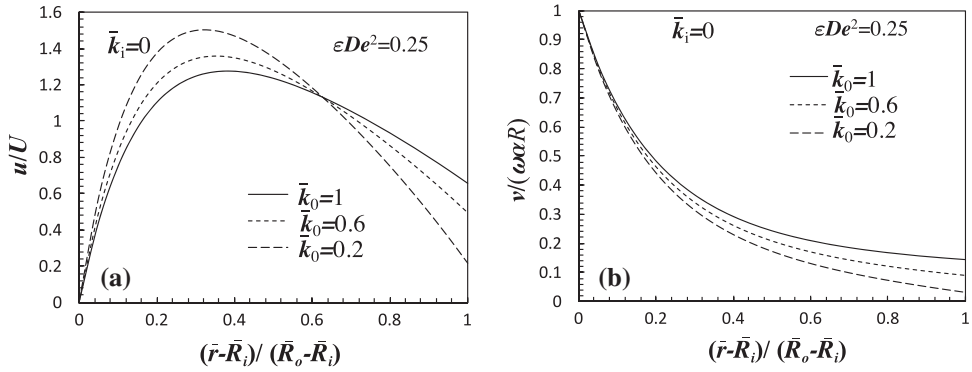

Fig. 14. Velocity profiles for the rotational dominant $\left(\frac{\omega\alpha R}{U}=20\right)$ flow of the linear PTT model with $\alpha=0.5,\ \varepsilon De^2=0.25, \bar{k}_i=0$ and a varying slip coefficient $\bar{k}_0=0.2, 0.6$ and 1 $\left(Re=10^3,\ Ta=10^8\right)$.

annulus for the higher slip coefficients. For the dimensionless velocity profile $\bar{u}$, Fig. 14(a) shows that the fluid also slips at the outer wall in the z direction. Several different flows could also be obtained assuming the cylinders have surfaces with different patterns in the z and θ directions. For these cases no analytical solution exists, and the non-linear system of governing equations needs to be solved numerically. In any case the overall pattern is that slip enhances flow in the axial direction, but in the tangential direction there is wall velocity enhancement only if there is slip at the outer wall, whereas slip at the driving inner cylinder reduces locally the velocity in the tangential direction.

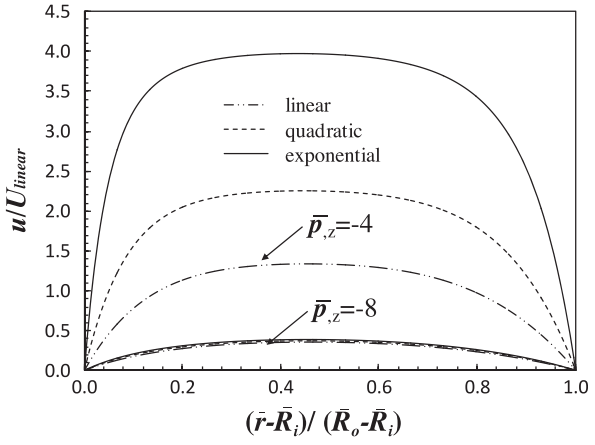

Fig. 15. Dimensionless velocity profiles for the linear, quadratic and exponential PTT models with $\alpha=0.5,\ \bar{k}=0$ and two different values of the dimensionless pressure drop, $\bar{p}_{,z}=-8$ and -4 for the linear PTT model (U_{linear} stands for the mean velocity obtained for the linear model and $\bar{p}_{,z}=-4$). The quadratic and exponential PTT model profiles were obtained for the same dimensional parameters of the linear PTT model.

4.2. Exponential PTT model

In order to compare the three models, Fig. 15 shows the velocity profiles obtained for two imposed dimensionless pressure drops, $\bar{p}_{,z}=-8$ and -4. We can see that for $\bar{p}_{,z}=-8$ (lower De) the velocity profiles are similar, but when $\bar{p}_{,z}$ decreases (in absolute value) higher velocities are obtained for the exponential model and smaller for the linear model, because for the same pressure gradient the flow rate is higher for the less viscous fluids, on account of the different shear-thinning behavior of the three models. The quadratic model behavior is in-between the linear and exponential models, as expected (c.f. Fig. 1).

5. Conclusions

Analytical solutions for the annular flow of linear and quadratic viscoelastic models were presented with and without wall slip. We found that for a constant flow rate the quadratic PTT model shows a more pronounced plug velocity profile and smaller shear and normal dimensionless extra-stress components, when compared to the linear model. Assuming the same slip coefficient at both walls, the presence of slip velocity brings the position of the null shear stress towards the inner cylinder. The numerical solution of the fully developed annular flow of the exponential PTT model was presented assuming an imposed pressure gradient, and this allowed the comparative study of the rheology of the three

constitutive models. For the helical flow we found that the presence of rotational flow and wall slip both change the linear and quadratic PTT models' behavior.

Acknowledgements

The authors gratefully acknowledge funding by COMPETE, FEDER and Fundação para a Ciência e a Tecnologia (FCT) through projects PEst-C/CTM/LA0025/2013 (Strategic Project – LA 25 – 2013-2014), PTDC/EQU-FTT/113811/2009 and PTDC/EME-MFE/113988/2009. LLF and AMA would also like to thank FCT for financial support through the scholarships SFRH/BD/37586/2007 and SFRH/BPD/75436/2010, respectively.

Appendix A. Pure axial annular flow of the quadratic PTT model

We assume the flow between the two concentric cylinders is fully developed, with the velocity component in the z direction only depending on the radial coordinate, r. We also assume that the outer and inner cylinders are both stationary. We remind that $\chi = 1$ for the quadratic model but if $\chi = 0$ the linear PTT solution is recovered.

The velocity profile for pure axial flow is given by,

$$\begin{aligned}\bar{u}(\bar{r}) = {} & \frac{\bar{p}_{,z}\left(\bar{r}^6 - 2\beta^2\bar{r}^4\overline{R}^2\ln(\bar{r})\right)}{4\bar{r}^4} - \frac{\bar{p}_{,z}\left(\alpha^6\overline{R}^6 - 2\alpha^4\beta^2\overline{R}^6\ln(\alpha\overline{R})\right)}{4\alpha^4\overline{R}^4} + \frac{De^2\varepsilon\bar{p}_{,z}^3\left(\bar{r}^6 - 6\beta^2\bar{r}^4\overline{R}^2 + 12\beta^4\bar{r}^2\overline{R}^4\ln(\bar{r}) + 2\beta^6\overline{R}^6\right)}{16\bar{r}^2} \\ & - \frac{\varepsilon De^2\bar{p}_{,z}^3\left(\alpha^6\overline{R}^6 - 6\alpha^4\beta^2\overline{R}^6 + 12\alpha^2\beta^4\overline{R}^6\ln(\alpha\overline{R}) + 2\beta^6\overline{R}^6\right)}{16\alpha^2\overline{R}^2} + \bar{k}_i\left(\frac{-\beta\overline{R}\bar{p}_{,z}}{2}\left(\frac{\beta}{\alpha} - \frac{\alpha}{\beta}\right)\right)^{m_i} \\ & + \frac{De^4\varepsilon^2\chi\bar{p}_{,z}^5\left(2\bar{r}^{10} - 15\beta^2\bar{r}^8\overline{R}^2 + 60\beta^4\bar{r}^6\overline{R}^4 - 120\beta^6\bar{r}^4\overline{R}^6\ln(\bar{r}) - 30\beta^8\bar{r}^2\overline{R}^8 + 3\beta^{10}\overline{R}^{10}\right)}{192\bar{r}^4} \\ & - \frac{De^4\varepsilon^2\chi\bar{p}_{,z}^5\left(2\alpha^{10}\overline{R}^{10} - 15\alpha^8\beta^2\overline{R}^{10} + 60\alpha^6\beta^4\overline{R}^{10} - 120\alpha^4\beta^6\overline{R}^{10}\ln(\alpha\overline{R}) - 30\alpha^2\beta^8\overline{R}^{10} + 3\beta^{10}\overline{R}^{10}\right)}{192\alpha^4\overline{R}^4}\end{aligned} \tag{A.1}$$

and the equation for the constant β is given by

$$\begin{aligned}& a\beta^{10} + b\beta^8 + c\beta^6 + d\beta^4 + e\beta^2 + f + \bar{k}_i\left[\frac{-\bar{p}_{,z}\beta\overline{R}}{2}\left(\frac{\beta}{\alpha} - \frac{\alpha}{\beta}\right)\right]^{m_i} \\ & \quad - \bar{k}_o\left[\frac{\bar{p}_{,z}\beta\overline{R}}{2}\left(\beta - \frac{1}{\beta}\right)\right]^{m_o} = 0\end{aligned} \tag{A.2}$$

where

$$\begin{aligned}a &= \varepsilon^2 De^4\overline{R}^6\chi\left(\frac{\bar{p}_{,z}^5}{64} - \frac{\bar{p}_{,z}^5}{64\alpha^4}\right) \\ b &= 5\varepsilon^2 De^4\overline{R}^6\chi\left(\frac{\bar{p}_{,z}^5}{32\alpha^2} - \frac{\bar{p}_{,z}^5}{32}\right) \\ c &= \frac{5\varepsilon^2 De^4\overline{R}^6\chi\bar{p}_{,z}^5\ln(\alpha)}{8} + \varepsilon De^2\overline{R}^4\bar{p}_{,z}^3\left(\frac{1}{8} - \frac{1}{8\alpha^2}\right) \\ d &= \varepsilon^2 De^4\overline{R}^6\chi\left(-\frac{5\alpha^2\bar{p}_{,z}^5}{16} + \frac{5\bar{p}_{,z}^5}{16}\right) - \frac{3\ln(\alpha)\varepsilon De^2\overline{R}^4\bar{p}_{,z}^3}{4} \\ e &= \varepsilon^2 De^4\overline{R}^6\chi\bar{p}_{,z}^5\left(\frac{5\alpha^4}{64} - \frac{5}{64}\right) + \varepsilon De^2\overline{R}^4\bar{p}_{,z}^3\left(\frac{3\alpha^2}{8} - \frac{3}{8}\right) + \frac{\overline{R}^2\bar{p}_{,z}\ln(\alpha)}{2} \\ f &= \varepsilon^2 De^4\overline{R}^6\chi\bar{p}_{,z}^5\left(\frac{1}{96} - \frac{\alpha^6}{96}\right) + \varepsilon De^2\overline{R}^4\bar{p}_{,z}^3\left(\frac{1}{16} - \frac{\alpha^4}{16}\right) - \frac{\alpha^2\overline{R}^2\bar{p}_{,z}}{4} + \frac{\overline{R}^2\bar{p}_{,z}}{4}\end{aligned} \tag{A.3}$$

For $\chi = 0$ (linear PTT model) and $m_i = 1, 2, 3$ Eq. (A.2) is further simplified and the solution is given by Eq. (29) with a_1, a_2 and a_3 given by Eqs. (30)–(32) (note that this equation does not depend on U if written in dimensional form).

For the solution of the direct problem (to determine the pressure gradient for a given flow rate) the following equation must be solved for $\bar{p}_{,z}$,

$$\chi d_1\bar{p}_{,z}^5 + d_2\bar{p}_{,z}^3 + d_3\bar{p}_{,z} + d_4(-\bar{p}_{,z})^{m_i} - \left(1 - \alpha^2\right) = 0 \tag{A.4}$$

where

$$\begin{aligned}d_1 &= \varepsilon^2 De^4\left(\frac{\overline{R}^6}{384} - \frac{\alpha^6\overline{R}^6}{96} + \frac{\alpha^8\overline{R}^6}{128} - \frac{5\beta^2\overline{R}^6}{192} + \frac{5\alpha^4\beta^2\overline{R}^6}{64} - \frac{5\alpha^6\beta^2\overline{R}^6}{96} + \frac{5\beta^4\overline{R}^6}{32} - \frac{5\alpha^2\beta^4\overline{R}^6}{16}\right) + \\ & \quad \varepsilon^2 De^4\left(\frac{5\alpha^4\beta^4\overline{R}^6}{32} + \frac{5\beta^6\overline{R}^6}{16} - \frac{5\alpha^2\beta^6\overline{R}^6}{16} - \frac{5\beta^8\overline{R}^6}{32} + \frac{5\beta^8\overline{R}^6}{32\alpha^2} - \frac{\beta^{10}\overline{R}^6}{64} - \frac{\beta^{10}\overline{R}^6}{64\alpha^4} + \frac{\beta^{10}\overline{R}^6}{32\alpha^2}\right) + \\ & \quad \varepsilon^2 De^4\left(\frac{5\beta^8\overline{R}^6\ln(\alpha)}{16} + \frac{5\beta^6\overline{R}^6\ln(\alpha)}{8}\right) \\ d_2 &= \varepsilon De^2\left(\frac{\overline{R}^4}{48} - \frac{\alpha^4\overline{R}^4}{16} + \frac{\alpha^6\overline{R}^4}{24} - \frac{3\beta^2\overline{R}^4}{16} + \frac{3\alpha^2\beta^2\overline{R}^4}{8} - \frac{3\alpha^4\beta^2\overline{R}^4}{16} - \frac{3\beta^4\overline{R}^4}{8} + \frac{3\alpha^2\beta^4\overline{R}^4}{8} + \frac{\beta^6\overline{R}^4}{8} - \frac{\beta^6\overline{R}^4}{8\alpha^2}\right) + \\ & \quad \varepsilon De^2\left(-\frac{\beta^6\overline{R}^4\ln(\alpha)}{4} - \frac{3\beta^4\overline{R}^4\ln(\alpha)}{4}\right) \\ d_3 &= \frac{\overline{R}^2}{8} - \frac{\alpha^2\overline{R}^2}{4} + \frac{\alpha^4\overline{R}^2}{8} + \frac{\beta^2\overline{R}^2}{4} - \frac{\alpha^2\beta^2\overline{R}^2}{4} + \frac{\beta^2\overline{R}^2\ln(\alpha)}{2} \\ d_4 &= \bar{k}_i\left[\frac{(\beta^2 - \alpha^2)\overline{R}}{2\alpha}\right]^{m_i}\left(1 - \alpha^2\right)\end{aligned} \tag{A.5}$$

The coefficients of this equation depend nonlinearly on β. Therefore, in order to solve the direct problem, we need to use an iterative procedure to solve the system of Eqs. (A.2) and (A.4) and obtain the pair $(\bar{p}_{,z}, \beta)$.

References

[1] N. Phan-Thien, R.I. Tanner, A new constitutive equation derived from network theory, J. Non-Newton. Fluid Mech. 2 (1977) 353–365.
[2] N. Phan-Thien, Influence of wall slip on extrudate swell: a boundary element investigation, J. Non-Newton. Fluid Mech. 26 (1988) 327–340.
[3] C.L.M.H. Navier, Sur les lois du mouvement des fluids, Mem. Acad. Roy. Sci. Inst. Fr. 6 (1827) 389–440.
[4] W.R. Schowalter, The behavior of complex fluids at solid boundaries, J. Non-Newton. Fluid Mech. 29 (1988) 25–36.
[5] M.P. Escudier, P.J. Oliveira, F.T. Pinho, Fully developed laminar flow of purely viscous non-Newtonian liquids through annuli, including the effects of eccentricity and inner-cylinder rotation, Int. J. Heat Fluid Flow 23 (2002) 52–73.
[6] M.P. Escudier, P.J. Oliveira, F.T. Pinho, S. Smith, Fully developed laminar flow of non-Newtonian liquids through annuli: comparison of numerical calculations with experiments, Exp. Fluids 33 (2002) 101–111.
[7] M.T. Matthews, J.M. Hill, Newtonian flow with nonlinear Navier boundary condition, Acta Mech. 191 (2007) 195–217.
[8] P.A. Thompson, S.M. Troian, A general boundary condition for liquid flow at solid surfaces, Nature 389 (1997) 360–362.
[9] D.M. Kalyon, M. Malik, Axial laminar flow of viscoplastic fluids in a concentric annulus subject to wall slip, Rheol. Acta 51 (2012) 805–820.
[10] M. Chatzimina, G.C. Georgiou, K. Housiadas, S.G. Hatzikiriakos, Stability of the annular Poiseuille flow of a Newtonian liquid with slip along the walls, J. Non-Newton. Fluid Mech. 159 (2009) 1–9.
[11] P.K. Kulshrestha, Helical flow of an idealized elastico-viscous liquid (I), Z. Angew. Math. Phys. ZAMP 13 (1962) 553–561.
[12] R.K. Bhatnagar, Steady laminar flow of visco-elastic fluid through a pipe and through an annulus with suction or injection at the walls, J. Ind. Inst. Sci. 45 (1963) 126–151.
[13] B.Y. Ballal, R.S. Rivlin, Flow of a viscoelastic fluid between eccentric cylinders, Rheol. Acta 14 (1975) 484–492.
[14] B.Y. Ballal, R.S. Rivlin, Flow of a viscoelastic fluid between eccentric cylinders II. Fourth-order theory for longitudinal shearing flow, Rheol. Acta 14 (1975) 861–880.
[15] B.Y. Ballal, R.S. Rivlin, Flow of a viscoelastic fluid between eccentric rotating cylinders, Trans. Soc. Rheol. 20 (1976) 65–101.
[16] B.Y. Ballal, R.S. Rivlin, Flow of a viscoelastic fluid between eccentric cylinders II. Poiseuille Flow, Rheol. Acta 18 (1979) 311–322.
[17] A.N. Beris, R.C. Armstrong, R.A. Brown, Perturbation theory for viscoelastic fluids between eccentric rotating cylinders, J. Non-Newton. Fluid Mech. 13 (1983) 109–143.
[18] F.T. Pinho, P.J. Oliveira, Axial annular flow of a nonlinear viscoelastic fluid – an analytical solution, J. Non-Newton. Fluid Mech. 93 (2000) 325.
[19] D.O. Cruz, F.T. Pinho, Skewed Poiseuille–Couette flows of SPTT fluids in concentric annuli and channels, J. Non-Newton. Fluid Mech. 121 (2004) 1–14.
[20] W.P. Wood, Transient viscoelastic helical flows in pipes of circular and annular cross-section, J. Non-Newton. Fluid Mech. 100 (2001) 115–126.
[21] M. Jamil, C. Fetecau, Helical flows of Maxwell fluid between coaxial cylinders with given shear stresses on the boundary, Nonlinear Anal.: Real World Appl. 11 (2010) 4302–4311.
[22] R. Bandelli, K.R. Rajagopal, Start-up flows of second grade fluids in domains with one finite dimension, Int. J. Non-Linear Mech. 30 (1995) 817–839.
[23] S. Wang, M. Xu, Axial Couette flow of two kinds of fractional viscoelastic fluids in an annulus, Nonlinear Anal.: Real World Appl. 10 (2009) 1087–1096.
[24] D. Tong, X. Zhang, Xinhong Zhang, Unsteady helical flows of a generalized Oldroyd-B fluid, J. Non-Newton. Fluid Mech. 156 (2009) 75–83.
[25] H. Qi, H. Jin, Unsteady helical flow of a generalized Oldroyd-B fluid with fractional derivative, Nonlinear Anal. RWA 10 (2009) 2700–2708.
[26] A.N. Beris, R.C. Armstrong, R.A. Brown, Spectral/finite-element calculations of the flow of a Maxwell fluid between eccentric rotating cylinders, J. Non-Newton. Fluid Mech. 22 (1987) 129–167.
[27] D. Rajagopalan, J.A. Byars, R.C. Armstrong, R.A. Brown, J.S. Lee, G.G. Fuller, Comparison of numerical simulations and birefringence measurements in viscoelastic flow between eccentric rotating cylinders, J. Rheol. 36 (1992) 1349–1375.
[28] X. Huang, N. Phan-Thien, R.I. Tanner, Viscoelastic flow between eccentric rotating cylinders: unstructured control volume method, J. Non-Newton. Fluid Mech. 64 (1996) 71–92.
[29] Y. Otsuki, T. Kajiwara, K. Funatsu, Numerical simulations of annular extrudate swell using various types of viscoelastic models, Polym. Eng. Sci. 39 (1999) 1969–1981.
[30] X.L. Luo, E. Mitsoulis, Memory phenomena in extrudate swell simulations for annular dies, J. Rheol. 33 (1989) 1307–1328.
[31] I. Mutlu, P. Townsend, M.F. Webster, Simulation of cable-coating viscoelastic flows with coupled and decoupled schemes, J. Non-Newton. Fluid Mech. 74 (1998) 1–23.
[32] R.G. Owens, T.N. Phillips, Computational Rheology, Imperial College Press, London, 2002.
[33] M.A. Alves, P.J. Oliveira, F.T. Pinho, Benchmark solutions for the flow of Oldroyd-B and PTT fluids in planar contractions, J. Non-Newton. Fluid Mech. 110 (2003) 45–74.
[34] J. Azaiez, R. Guénette, A. Aitkadi, Numerical simulation of viscoelastic flows through a planar contraction, J. Non-Newton. Fluid Mech. 62 (1996) 253–277.
[35] L.L. Ferrás, J.M. Nóbrega, F.T. Pinho, Analytical solutions for Newtonian and inelastic non-Newtonian flows with wall slip, J. Non-Newton. Fluid Mech. 175–176 (2012) 76–88.